Earth and Planetary Science Letters 390 (2014) 8–18

Contents lists available at ScienceDirect

Earth and Planetary Science Letters

www.elsevier.com/locate/epsl

Dating the Homo erectus bearing travertine from Kocabaş (Denizli, Turkey) at at least 1.1 Ma

Anne-Elisabeth Lebatard [a,*], M. Cihat Alçiçek [b], Pierre Rochette [a], Samir Khatib [c], Amélie Vialet [d], Nicolas Boulbes [e], Didier L. Bourlès [a,*], François Demory [a], Gaspard Guipert [f], Serdar Mayda [g], Vadim V. Titov [h], Laurence Vidal [a], Henry de Lumley [i]

[a] Aix-Marseille Université, CNRS-IRD-Collège de France, UM 34 CEREGE, Technopôle de l'Environnement Arbois-Méditerrannée, BP80, 13545 Aix-en-Provence, France
[b] Department of Geology, Pamukkale University, 20070 Denizli, Turkey
[c] Laboratoire départemental de Préhistoire du Lazaret, Conseil Général des Alpes-Maritimes, UMR 5198 CNRS, Parc de la Villa La Côte, 33 bis, boulevard Franck Pilatte, 06300 Nice, France
[d] Département de Préhistoire du Muséum National d'Histoire Naturelle, UMR 7194 du CNRS, Institut de Paléontologie Humaine, 1 rue René Panhard, 75013 Paris, France
[e] EPCC, Centre Européen de Recherches Préhistoriques, Avenue Léon-Grégory, 66720 Tautavel, France
[f] Antenne de l'Institut de Paléontologie Humaine, CEREGE, Technopôle de l'Arbois, bâtiment Villemin, BP80, 13545 Aix-en-Provence, France
[g] Natural History Museum, Ege University, 35100 Bornova, Izmir, Turkey
[h] Institute of Arid zones SSC RAS, Chekhov str., 41, Rostov-on-Don, Russia
[i] Institut de Paléontologie Humaine, Fondation Albert 1er, Prince de Monaco, 1, Rue René Panhard, 75013 Paris, France

ARTICLE INFO

Article history:
Received 15 July 2013
Received in revised form 10 December 2013
Accepted 23 December 2013
Available online 17 January 2014
Editor: B. Marty

Keywords:
Cosmogenic nuclide
Burial dating
Paleomagnetism
Homo erectus
Villafranchian

ABSTRACT

Since its discovery within a travertine quarry, the fragmentary cranium of the only known Turkish *Homo erectus*, the Kocabaş hominid, has led to conflicting biochronological estimations. First estimated to be ~500 ka old, the partial skull presents a combination of archaic and evolved features that puts it as an intermediate specimen between the Dmanisi fossils (*Homo georgicus*) and the Chinese Zhoukoudian skulls (*Homo erectus*) respectively dated to 1.8 to ~0.8 Ma. Here we present a multidisciplinary study combining sedimentological, paleontological and paleoanthropological observations together with cosmogenic nuclide concentration and paleomagnetic measurements to provide an absolute chronological framework for the Upper fossiliferous Travertine unit where the Kocabaş hominid and fauna were discovered. The $^{26}Al/^{10}Be$ burial ages determined on pebbles from conglomeratic levels framing the Upper fossiliferous Travertine unit, which exhibits an inverse polarity, constrains its deposition to before the Cobb Mountain sub-chron, that is between 1.22 and ~1.5 Ma. The alternative match of the normal polarity recorded above the travertine with the Jaramillo subchron (lower limit 1.07 Ma) may also be marginally compatible with cosmogenic nuclides interpretation, thus the proposed minimum age of 1.1 Ma for the end of massive travertine deposition. The actual age of the fossils is likely to be in the 1.1–1.3 Ma range. This absolute date is in close agreement with the paleoanthropological conclusions based on morphometric comparisons implying that Kocabaş hominid belongs to the *Homo erectus s.l.* group that includes Chinese and African fossils, and is different from Middle and Upper Pleistocene specimens. Furthermore, this date is confirmed by the large mammal assemblage, typical of the late Villafranchian. Because it attests to the antiquity of human occupation of the Anatolian Peninsula and one of the waves of settlements out of Africa, this work challenges the current knowledge of the *Homo erectus* dispersal over Eurasia.

1. Introduction

The Denizli basin (Fig. 1(a)), one of the Neogene extensional depressions of western Anatolia (Westaway, 1993), contains important travertine formations massively mined by marble industries. This intensive activity has brought to light from the Upper formation of Kocabaş travertines fossiliferous remains of large mammals among which one of us (M.C. Alçiçek) discovered a fragmentary

* Corresponding authors.
E-mail addresses: lebatard@cerege.fr (A.-E. Lebatard), bourles@cerege.fr (D.L. Bourlès).

http://dx.doi.org/10.1016/j.epsl.2013.12.031
0012-821X

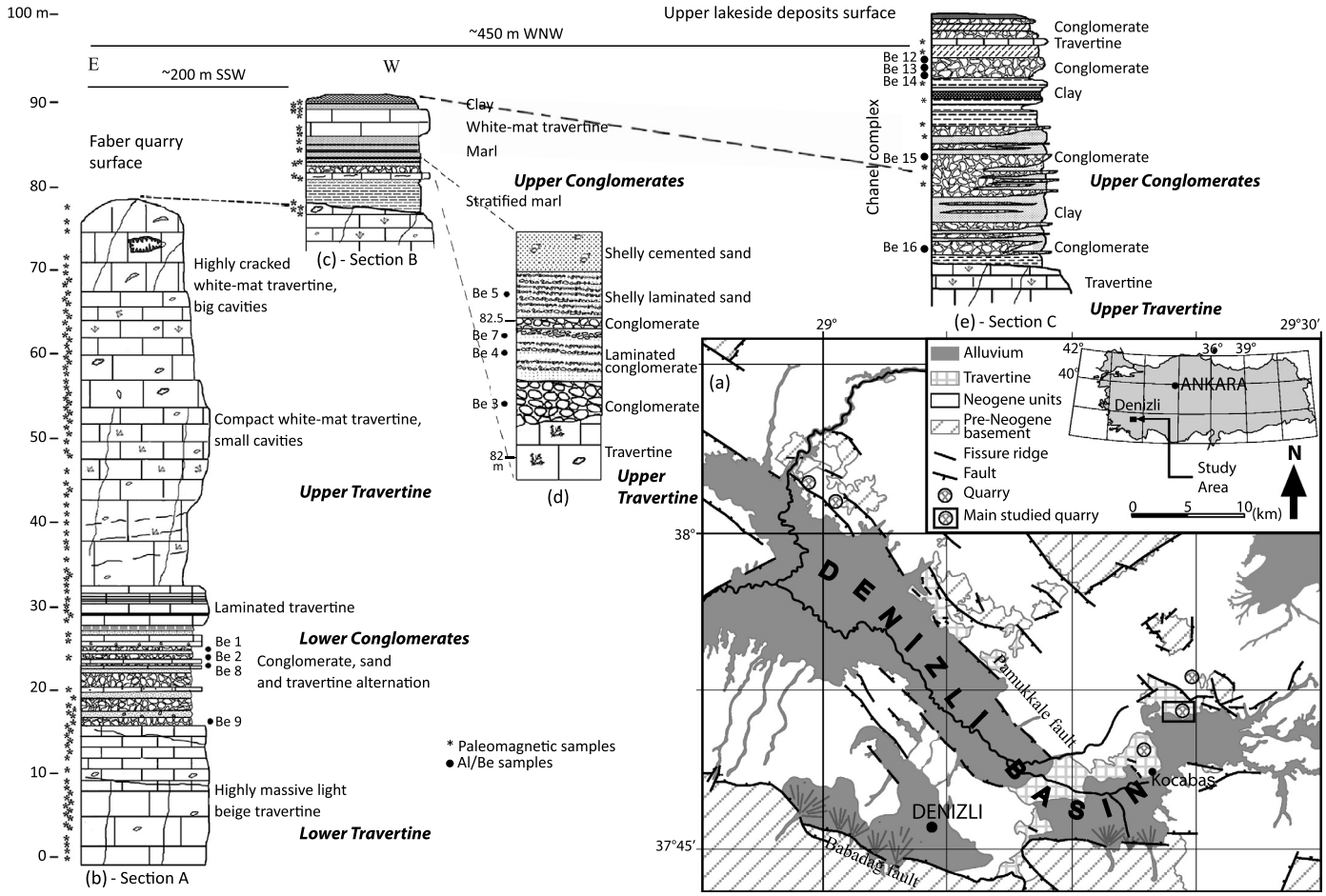

Fig. 1. Sample location around the Faber quarry, Kocabaş, Denizli, Turkey. (a) Geological map of Denizli basin (based on Sun, 1990); (b) Section A, travertine stratigraphic section in the Faber quarry (Fig. S5=mmc5); (c) Section B, upper fluvio-lacustrine stratigraphic section in the Faber quarry SW wall (Upper Conglomerates; Fig. S5=mmc5); (d) detail of the (c) stratigraphic section (between 81.9 m and 82.8 m of height); (e) Section C, upper fluvio-lacustrine stratigraphic section west of the Faber quarry (2012 samples in green in Fig. S5=mmc5).

Homo erectus cranium in 2002, as reported by Kappelman et al. (2008). The earliest age determination of the travertines in Kocabaş field at 1.11 ± 0.11 Ma was performed by Engin et al. (1999) using Electron Spin Resonance method, but a circa 500 ka date using thermoluminescence method was also reported (Kappelman et al., 2008). However, both methods are at the limits of their applicability and may suffer various unconstrained biases.

The partial skull of the only known Turkish *Homo erectus*, the Kocabaş hominid, presents an intermediate morphological pattern (Vialet et al., 2012) between the *Homo* skulls from Dmanissi (Georgia) and those from Zhoukoudian Lower-cave (China) dated, at 1.8 Ma (de Lumley et al., 2002) and at ~0.8 Ma (Shen et al., 2009), respectively. Furthermore, previous studies of the fauna found in the same level (i.e. Upper Travertine) points toward common Middle Pleistocene species (Erten et al., 2005). Note that the faunal assemblage used in the paleontological present study is more complete.

Because Kocabaş hominid has been discovered on an alternative species migration pathway between Europe and Asia (Bar-Yosef and Belmaker, 2011), it is of fundamental importance to secure these conflicting biochronological estimations to provide an absolute chronological framework for the Kocabaş hominid and the Upper Travertine level fauna. As in Zhoukoudian (China; Shen et al., 2009), and Attirampakam (India; Pappu et al., 2011), a multidisciplinary approach combining extensive sedimentological studies, paleomagnetism, determination of the paleo-mammal fauna and their paleo-biodiversity and cosmogenic nuclide concentration measurements has thus been carried out. A new 3D reconstruction of the fragmentary skull enabled further anthropological comparisons with the fossil record.

2. Settings

2.1. Geological context of the studied section and hominid remains discovery

Located in one of the world's most seismically active regions, at the junction between the E-W-trending Büyük Menderes and the NW-SE-trending Gediz Graben (Bozkurt, 2001), the Denizli Basin (Fig. 1(a)) is a fault bounded Neogene-Quaternary depression in the west Anatolian extensional province. From a half graben controlled by the south Babadağ fault zone during the late-Early Miocene, the depression turned into a graben due to the activation of the north Pamukkale fault zone resulting from changes of the regional extensional directions during the early Quaternary (Alçiçek et al., 2007). Dip-slip normal fault segments displaying step-over zones along the fault-strikes (e.g. Hancock et al., 1999) governed hot spring resurgences that precipitate massive travertine deposits mainly along the northern margin of the basin, which includes the studied Kocabaş travertine field (Şimşek et al., 2000).

The fossil travertine field of Kocabaş is deformed and exposed along NW-trending normal faults to the east of Denizli basin. Starting during the Roman period, quarrying significantly intensified since the late 1990s for commercial purposes. The quarries are

located along the strike of the travertine exposures and in each excavation the fossil bearing horizons are located at the top of the travertine mass.

As reported by Kappelman et al. (2008), the *Homo* specimen was recovered from a block of travertine extracted from a quarry which was rented by G. Vurdaal, owner of the factory where the fossil was cut. One of us (M.C. Alçiçek), engaged in a systematic search for fossils, obtained the specimen directly from the factory owner within a few weeks after slicing and recognized it as an hominid remain. Direct interview with G. Vurdaal confirmed that the block came from one of the quarries installed on a continuous travertine dome, whose centre is excavated by the Faber quarry. In the Kocabaş travertine field, the Faber quarry is the one that allows continuous sampling over the longest travertine sequence and associated detrital sediments. Therefore it was chosen for stratigraphic sampling while adjacent quarries were also sampled. Although dating the Faber quarry travertine does not ipso facto precisely place the hominid in a firm chronology, evidences that the hominid predates the end of travertine formation in this area are compelling. The provenance of the hominid remains in the Upper Travertine is inferred from the fact that in 2002 the excavations were limited to this upper formation.

2.2. Paleontological background

Mammals' remains come mainly from the upper part of travertines deposits (Upper Travertine) in the Kocabaş area. Fossils are found during the slicing of travertine blocks for commercial purpose. The fossils are embedded within strongly consolidated travertines and therefore almost impossible to release from the host rock. They are in consequence badly preserved and difficult to study. Since Erten et al. (2005), the updated faunal list includes the following species: *Archidiskodon meridionalis meridionalis*, *Equus* middle to large form (affinities with E. *apolloniensis-suessenbornensis*), *Equus* cf. *altidens*, *Stephanorhinus* cf. *etruscus*, *Metacervoceros rhenanus*, *Cervalces* (*Libralces*) ex gr. *minor-gallicus*, *Palaeotragus* sp., Bovinae gen. indet. (Fig. S1=mmc1).

In the composition of the taphocenosis, forms common to Early Pleistocene are present. In particular the characteristics of the southern elephant teeth are typical for early-middle late Villafranchian form. Etruscan rhino and the dama-like deer genera Metacervoceros are also classic elements of Villafranchian fauna. The very small elk and giraffe are unknown later than ~1.5 Ma in Europe and neighboring regions. There is only one Greek locality (Q-Profil) with findings of similar giraffe whose age was determined to be around 1.2 Ma (van der Made and Morales, 2011). Two species of equids were ascribed to forms possessing rather archaic and progressive features with a wide stratigraphic distribution – from the Early Pleistocene to early Middle Pleistocene. Generically, this association resembles those from the late Villafranchian of Southern and Eastern Europe, and, partly, from Western Asia (Kahlke et al., 2011), i.e. older than 1 Ma.

2.3. Paleoanthropological setting

The Kocabaş skull comprised three fragments belonging to the same individual (Fig. S2=mmc2): a fragment of the right part of the frontal bone, the anterior half of the right parietal bone and two left frontal and parietal fragments still connected. A first virtual reconstruction re-established the anatomical connection between the three cranial remains (Vialet et al., 2012). A more recent 3D reconstruction, carried out to adjust the location of the right frontal part with the rest of the fragmentary skull, leads to a more confident 3D reconstruction (Fig. 2).

Morphological and metrical comparisons between the Kocabaş skull and other Pleistocene specimens from Africa, Asia and Europe

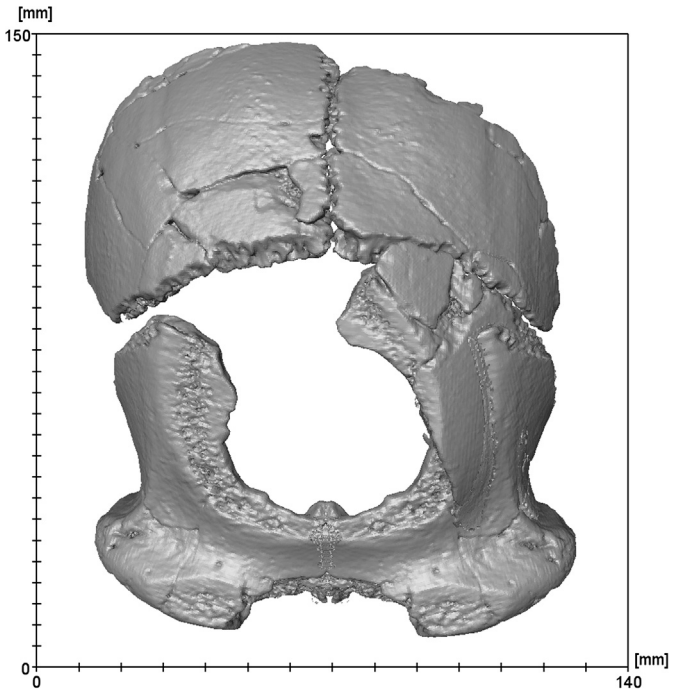

Fig. 2. 3D reconstruction of the Kocabaş fragmentary skull, connecting the two parietal bones and completing the left anterior (supratoral) frontal area by mirroring the right part which is preserved. Note that there is no strict anatomical link between the right part of the frontal and the right parietal bones because of some lacks in the suture area.

focused on the frontal bone almost complete on the reconstructed Turkish fossil (Vialet et al., 2012). Regarding the anatomy and size of the anterior part of the frontal bone, they indicate that the Kocabaş specimen is similar to the African specimens ER3733 and OH9 as well as to the Chinese fossils from Zhoukoudian L-C and Hulu cave (Nankin 1) but clearly distinct from the more archaic fossils from Dmanisi in Georgia, on one hand, and from the Middle and Upper Pleistocene specimens, on the other hand. Temporal lines are in a higher location on the Georgian fossils and there is no more bulge on the temporal area of the frontal on the recent ones.

Moreover, the Kocabaş frontal bone, considering the minimum frontal breadth and the length from the post-glabellar sulcus to bregma (Fig. S3=mmc3) differs in proportion from that of the Zhoukoudian L-C and Sangiran 17 (Java) fossils, which are as large as the Turkish fossil but longer. In addition, Kocabaş frontal scale is distinct from those of the ER3733 and Bouri–Daka specimens, which are shorter, and from those of OH9 which are slightly larger and longer.

Morphometrics (Fig. S4=mmc4) confirm these results. The principal components analysis performed via Morphologika2, based on the covariance matrix of the Procrustes residuals (after a Procrustes Superimposition of the specimens included in the analysis), shows that Kocabaş clearly belongs to the *Homo erectus s.l.* group including fossils from Africa, China and Georgia (*Homo georgicus*). It is different from the Indonesian *Homo erectus* and Middle and Upper Pleistocene specimens (*Homo heidelbergensis*, Neandertals and Upper Palaeolithic *Homo sapiens*). The Turkish fossil closely matches African specimens such as ER3733 and OH9.

3. Sampling

As explained above, we chose the longest and more complete sequence available. Three sections from the Faber quarry and an adjacent quarry (N 37°52′3″, E 29°20′17″; Supplementary KMZ file=mmc8) have been investigated in detail: A – a 93 m high

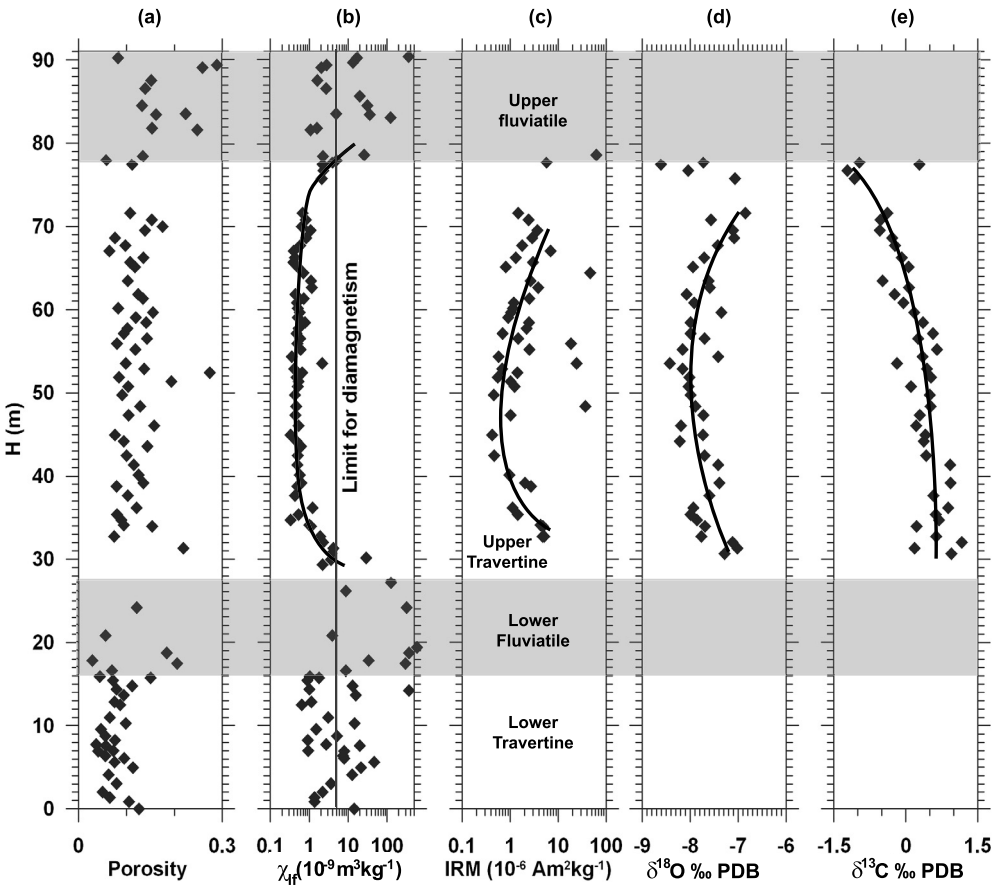

Fig. 3. Log of different parameters as a function of the stratigraphic height along sections A and B. (a) Porosity obtained using bulk density measurement of paleomagnetic cylinder, and grain density of 2.66 ± 0.03 measured on 20 samples with the helium pycnometer; (b) magnetic susceptibility measured with MFK1 corrected from a pure calcite susceptibility of $4.8 \cdot 10^{-9}$ $m^3\,kg^{-1}$; (c) saturation remanence (IRM) acquired in a 3 T field; (d) and (e) oxygen and carbon isotopic composition expressed in δ‰ versus PDB, respectively. Measured isotopic values are normalized against the international standard NBS-19. Mean external reproducibility was better than 0.03‰ for $\delta^{13}C$ and 0.05‰ for $\delta^{18}O$.

(78 m of outcrops from the bottom of the quarry to the top of the hill plus a 15 m borehole drilled in the quarry bottom) continuous travertine section (Fig. 1(b)); B and C – 13 m (Fig. 1(c), (d)) and 30 m (Fig. 1(e)) thick sections in fluvio-lacustrine deposits (Upper Conglomerates) lying in unconformity at the top of the massive travertine formation. Both Upper Conglomerates sections (B and C) are ∼200 m and ∼450 m away from the travertine section (A). Continuous outcropping allows the A and B sections to be precisely correlated (Fig. 1, Fig. S5=mmc5 and Fig. S6=mmc6). The travertine formation termination has been sampled in four sites (sections A, B plus two separate outcrops in adjacent quarries; Fig. 1, Fig. S5=mmc5 and Fig. S6=mmc6).

Among the sampled massive travertine formation, 12 m of fluvio-lacustrine deposits (Lower Conglomerates) separate a lower massive light beige travertine formation from an upper more porous white mat travertine formation (Fig. 1(b)). Sampled travertine comprised 97 to 99 wt.% calcite and 1 to 3% of <50 µm detrital silicated sediments. Average porosity in the Lower and Upper Travertine samples are 7 and 12%, respectively (Fig. 3). The grain-size distribution and the lithological composition of both the Upper and Lower Conglomerates are similar and typical of fluviatile input originating from the overlying hill catchments. Although mainly limestone, the pebbles may also be quartz and metamorphic rocks. The sand fraction (0.05 mm to 2 mm) contains approximately 65% calcium carbonate, 29% quartz, 2% feldspars and 4% lithic fragments of metamorphic origin. For the correlation of sections B and C (distant by 400 m), although there is not a continuous outcropping condition, the correlation we propose is based on a robust set of field evidences. First the elevation of the travertine base of section B matches (as seen by dip extrapolation in the landscape) with the one of the travertine base of section C. The facies of travertine observed at B and C bases are identical, and clearly different from the Lower Travertine of section A. The Lower Conglomerates of section A is well indurated, while the conglomerate of section C is very loose, just as the Upper Conglomerates of section B. The alternative correlation of section C with the Lower Conglomerates unit of section A is thus excluded. Relative stratigraphic height of C and B were matched versus the A section, using the top of the Upper Travertine formation as a tie point, allowing to obtain a composite section of 121 m. Possible lateral variation of deposition rate (especially between B and C) may introduce significant uncertainties in this relative match.

Paleomagnetic sampling was performed for a total of 165 samples at an interval of 0.5 to 1 m, except in detrital layers where sampling was not possible in the too coarse or loose layers, in particular the lower part of section C (Fig. 1). Most were obtain with a portable 25 mm corer with compass orientation except a few hand samples in unconsolidated layers, and the borehole samples obtained as fragments of the half 45 mm core, with length in the 10–20 cm range. Oriented samples were cut to standard cylinders (surface oriented core), cubes (hand samples) or bars (borehole) for natural remanent magnetization (NRM) measurement.

For cosmogenic nuclides measurement, four few kg samples resulting from the mixing of tens of centimetric to decametric quartz and ophiolitic clast pebbles have been taken in 2011 from each of the quartz-containing conglomerates units (Fig. 1, Fig. S5=mmc5

Table 1
Cosmogenic nuclide concentrations, burial ages and denudations rates of the Denizli samples.

Unit	Sample	W. dis. Qz (g)	H (m)	D (m)	^{10}Be (10^5 at g^{-1})	^{26}Al (10^5 at g^{-1})	Model without post-burial production		Model with post-burial production				Gr. min. burial age (Ma)
							Burial age (Ma)	Denudation before burial (m Ma^{-1})	Burial age (Ma)	Denudation before and after burial (m Ma^{-1})	Post-burial ^{10}Be produced (10^3 at g^{-1})	Post-burial ^{26}Al produced (10^3 at g^{-1})	
Lower Conglo.	DZ-Be-1	19.2	25.0	53.2	1.854 ± 0.060	5.041 ± 0.378	1.96 ± 0.16	9.4 ± 0.8	1.95 ± 0.16	10.8 ± 0.5	2.05	3.33	1.80
	DZ-Be-2	17.2	23.8	54.1	2.112 ± 0.067	2.904 ± 0.919	3.30 ± 1.05	3.8 ± 1.2	3.31 ± 1.05	4.4 ± 0.8	2.98	4.23	2.76
	DZ-Be-8	20.0	22.7	55.6	2.046 ± 0.065	6.005 ± 0.450	1.79 ± 0.15	9.2 ± 0.7	1.78 ± 0.15	10.5 ± 0.5	1.77	2.88	1.63
	DZ-Be-9	19.4	16.3	62.0	1.521 ± 0.049	3.548 ± 0.320	2.29 ± 0.22	9.7 ± 0.9	2.28 ± 0.22	11.1 ± 0.6	1.31	2.05	2.10
Upper Conglo.	DZ-Be-3	19.4	82.2	9.1	0.970 ± 0.051	3.747 ± 0.202	1.27 ± 0.10	29.4 ± 2.2	1.44 ± 0.11	31.6 ± 2.4	14.00	78.58	1.12
	DZ-Be-4	20.0	82.4	8.9	0.822 ± 0.037	2.746 ± 0.203	1.58 ± 0.14	29.7 ± 2.6	1.93 ± 0.17	30.6 ± 2.6	15.00	83.55	1.41
	DZ-Be-5	18.9	82.6	8.7	0.895 ± 0.042	3.253 ± 0.197	1.40 ± 0.11	29.8 ± 2.3	1.66 ± 0.13	31.4 ± 2.4	14.67	83.53	1.25
	DZ-Be-7	19.9	82.4	8.8	0.965 ± 0.036	3.737 ± 0.236	1.27 ± 0.09	29.5 ± 2.2	1.45 ± 0.11	31.7 ± 2.3	14.24	81.40	1.12
	DZ-Be-12	11.4		4.9	2.262 ± 0.072	7.999 ± 0.528	1.40 ± 0.10	11.1 ± 0.8	1.97 ± 0.15	9.8 ± 0.7	35.35	285.20	1.26
	DZ-Be-13	4.4		5.9	1.686 ± 0.094	6.553 ± 0.702	1.23 ± 0.15	16.7 ± 2.0	1.59 ± 0.19	16.3 ± 2.0	24.89	183.21	0.99
	DZ-Be-14	18.4		6.9	2.202 ± 0.069	7.425 ± 0.401	1.50 ± 0.09	10.8 ± 0.7	1.91 ± 0.12	10.2 ± 0.6	30.12	214.14	1.38
	DZ-Be-15	15.1		16.5	1.392 ± 0.045	4.864 ± 0.338	1.46 ± 0.11	18.1 ± 1.4	1.49 ± 0.12	19.7 ± 1.5	12.40	48.16	1.31
	DZ-Be-16	17.1		23.5	0.444 ± 0.024	1.448 ± 0.190	1.65 ± 0.24	54.0 ± 7.7	1.63 ± 0.23	60.4 ± 8.6	4.06	11.43	1.37

The "Model without post-burial production" assuming that the samples did not accumulate cosmogenic nuclides while buried (infinite burial depth) yields minimum burial age. The "Model with post-burial production" assuming for modeling that the samples remained buried at their sampling depths and accumulated cosmogenic nuclides produced by muons yields maximized burial ages. In this later case, denudation rate is considered equal before and after burial. Burial age and denudation rate uncertainties (reported as 1σ) propagate the half-life uncertainties. Neutronic production is 6.93 at g^{-1} a^{-1} for ^{10}Be and 45.83 at g^{-1} a^{-1} for ^{26}Al, slow muons production is 0.02 at g^{-1} a^{-1} for ^{10}Be and 1.12 at g^{-1} a^{-1} for ^{26}Al, and fast muons production is 0.05 at g^{-1} a^{-1} for ^{10}Be and 0.09 at g^{-1} a^{-1} for ^{26}Al (Braucher et al., 2011). Density of the travertine quarry part is 2.33 g cm^{-3} and 2.14 g cm^{-3} for the lakeside deposits. The chemical blank ratio are $2.13 \cdot 10^{-15}$ and $7.53 \cdot 10^{-16}$ for ^{10}Be/^{9}Be and ^{26}Al/^{27}Al ratio, respectively. The measured ratios are corrected from these values. Conglo. = conglomerates; W. dis. Qz = weight of dissolved quartz; H = stratigraphic height from quarry bottom; D = depth below the surface, both in meter; Gr. Min. burial age: Minimum burial age deduced from the exposure-burial diagram (Fig. 4). The graphically determined minimum burial ages were obtained considering the radioactive decay duration necessary to straightforwardly reach from the lower "steady erosion" curve of the "steady-state erosion island" the minimum ^{26}Al/^{10}Be ratio value considering the associated uncertainties.

and Fig. S6=mmc6, Table 1) in the Faber quarry. Five conglomeratic samples were also collected in 2012 in an adjacent quarry (section C, Fig. 1(e), Fig. S5, Table 1). The samples from the Lower and Upper Conglomerates are buried under 50 to 62 m and 8.7 to 9 m of overlying material (4.9 to 23.5 m for section C), respectively.

The paleontological field observations only revealed abundant plant and gastropod remains in the Upper Travertine and the Upper Conglomerates units. New large mammal remains available for this study were exclusively recovered by the quarry employees while processing blocks coming from the Upper Travertine unit. This is confirmed by the color, porosity, plant and gastropod remains perfect match between the mammal containing slabs and the in-situ observed formation.

4. Experimental methods

4.1. Paleomagnetic method

NRM of at least one specimen per oriented core or block was measured using a 2G DC-Squid Superconducting Rock Magnetometer (SRM), with noise level in the order of 10^{-6} A m^{-1}. The direction of characteristic remanent magnetization (ChRM) was retrieved by means of stepwise demagnetization using alternating field (AF, with the online 2G system) and/or heating (using a MMTD80 oven) and analyzing the demagnetization curve using principal component analysis. Magnetic susceptibility was measured on all samples using a MFK1 bridge and normalized by mass. Isothermal remanence (IRM) was acquired in a 3 T pulse field and measured with the 2G SRM, at different AF demagnetization steps, on a subset of 64 cores. A back field of 0.3 T was applied on the 3 T IRM to obtain the Sratio (ratio between the backfield and initial IRM) on a subset of 14 samples. Hysteresis loops and back field remanence curves were measured on chips of 6 samples using a Micromag 3900 VSM, with a 1 T maximum field. Bulk density and porosity was estimated by measuring total volume (cylinder dimension) and solid volume (by helium pycnometry). Carbon and oxygen isotopic composition of travertine carbonate was determined using a Delta Plus Advantage Thermo-Finnigan Spectrometer.

The consistent geomagnetic polarities indicated by ChRM directions were interpreted by comparison with the geomagnetic polarity timescale (GPTS, Laj and Channell, 2007 and references therein) using further constraint from cosmogenic nuclides and paleontology.

4.2. Cosmogenic nuclide method

The burial dating method is based on the radioactive decay of the two cosmogenic nuclides, ^{26}Al and ^{10}Be, produced within the quartz (SiO_2) mineral fraction (in-situ production) of rocks exposed at the Earth's surface. Due to spallation reactions induced by the secondary cosmic ray derived energetic particles on silicon (Si) and oxygen (O), both cosmogenic nuclides accumulate during surface exposure in the selected mineral fraction with a well constrained ^{26}Al/^{10}Be spallogenic production rate ratio of 6.61 ± 0.50 updated from the Nishiizumi original ratio (e.g. Nishiizumi et al., 1989; Rixhon et al., 2011; Pappu et al., 2011). The cosmic ray flux being efficiently attenuated by matter (e.g. Granger and Muzikar, 2001), the burial of previously exposed surfaces under a few meters of matter leads to a reduction of the effective energetic particle flux efficient enough to stop ^{26}Al and ^{10}Be production. Both cosmogenic nuclide accumulated concentrations therefore starts to radioactively decrease according to their respective half-lives, which is 0.717 ± 0.017 Ma for ^{26}Al (Samworth et al., 1972; Granger, 2006) and 1.387 ± 0.012 Ma for ^{10}Be (Korschinek et al., 2010; Chmeleff et al., 2010). ^{26}Al concentrations decrease roughly twice as fast as the ^{10}Be concentrations, the ^{26}Al/^{10}Be concentration ratio decreases exponentially with an apparent half-life of 1.48 ± 0.01 Ma. This offers the opportunity to determine the duration of burial episodes lasting from 100 ka up to 5 Ma (Granger and Muzikar, 2001).

The sample preparation and the AMS measurement procedure are fully described in Braucher et al. (2011). ^{26}Al and ^{10}Be concentrations having been measured in the same quartz sample, this insures that they both record the same exposition, denudation and burial history. The ^{26}Al and ^{10}Be concentrations are presented in Table 1. They yield a specific ^{26}Al/^{10}Be concentration ratio associated to each sample that allow the sample burial duration to be estimated. Uncertainties linked to the calculated concentrations, ages and denudation rates, are reported at 1σ and result from the propagation of the uncertainties linked to the measured concentrations and to the used half-lives.

Following the model fully described in the SOM of Pappu et al. (2011), burial ages and denudation rates were determined using the parameters discussed in Braucher et al. (2011), including the ^{26}Al/^{10}Be spallogenic production rate ratio of 6.61 ± 0.50. Neutronic production rates have been scaled using (Stone, 2000) and are based on a weighted mean spallation production rate at sea level and high latitude (SLHL) of 4.03 ± 0.18 at g^{-1} a^{-1} (Molliex et al., 2013) for the ^{10}Be obtained combining the more recent calibrated production rates in the northern hemisphere (Balco et al., 2009; Fenton et al., 2011; Goehring et al., 2012 and Briner et al., 2012).

Prior to their burial, the samples accumulate cosmogenic nuclide concentrations whose maximum values are determined assuming that the steady state between the gains through cosmogenic nuclide accumulation and the losses through denudation and radioactive decay has been reached (infinite surface exposure duration). This allows denudation rates before burial to be estimated (see SOM of Pappu et al., 2011). Calculated for each sample, these maximum cosmogenic nuclide concentrations and their associated denudation rates are used to compute a burial age and possible post-burial ^{10}Be and ^{26}Al concentrations (post-burial production).

Theoretically, considering a null post-burial production such as that implied by a burial fast and deep enough to efficiently stop cosmogenic nuclide production allows to determine a minimum burial age based on the sole differential cosmogenic nuclides radioactive decay and the estimated denudation rates (Table 1: "Model without post-burial production"). The determination of the minimum burial duration is based on a model shown in the exposure-burial diagram (Fig. 4; e.g. Granger, 2006) which aims to reproduce the minimum burial duration required to lead by radioactive decay from an initial ^{26}Al/^{10}Be concentration ratio conditioned by the denudation rate before burial to the measured ratio. The measured value may, however, also result from different and more complicated scenarios involving repeated burials and exposures and obviously leading to significantly longer burial duration.

If the burial is not thick enough to efficiently stop cosmogenic nuclides production then mainly due to muons, the cosmogenic nuclide concentrations measured in the samples correspond to the sum of the cosmogenic nuclide concentrations accumulated during the surface exposure that have undergone radioactive decay and of the cosmogenic nuclide concentrations accumulated during the burial period at the sampling depth. Then, the assumption that the environmental conditions remained relatively stable over the Pleistocene period and, thus, that the denudation rates remained similar before and after burial leads to a maximized burial age estimate (Table 1: "Model with post-burial production"). All burial ages, denudation rates and post-burial concentrations have been summarized in Table 1. The samples results are also plotted in the graph ^{26}Al/^{10}Be versus ^{10}Be (Fig. 4), also called "exposure-burial diagram" (e.g. Granger, 2006).

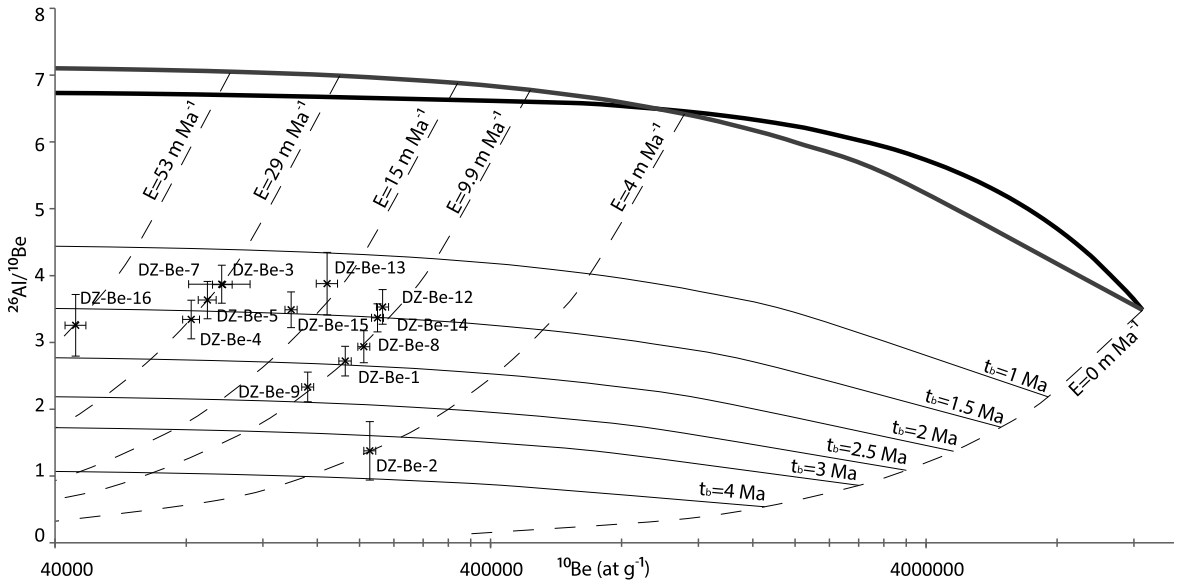

Fig. 4. $^{26}Al/^{10}Be$ ratio versus ^{10}Be concentration (e.g. Granger and Muzikar, 2001; Granger, 2006) for the Denizli conglomerates samples. The dark bold curve corresponds to a denudation equal to zero and a finite exposure time (constant exposure curve). The grey bold curve corresponds to a finite denudation with an infinite exposure time (steady denudation curve). The part below these two curves represents the burial area. Each thin dark curves represents a specific burial time (t_b), and each thin dashed dark curves corresponds to a denudation rate (E) in $m\,Ma^{-1}$. All the samples are plotted in the burial area with their associated uncertainties (see Table 1).

5. Results

5.1. Paleomagnetic study

Measured NRM intensities vary from a few 10^{-6} $A\,m^{-1}$ (i.e. just above noise level) to above 10^{-4} $A\,m^{-1}$. Low intensity characterizes the Upper Travertine unit, which is also characterized by diamagnetic susceptibility close to that of pure calcite (Fig. 3). AF and thermal NRM demagnetization behavior has been studied with 20 pilot samples (Fig. 5). Secondary magnetization in variable relative proportion is found to be mostly erased using heating above 150–200 °C and AF of a few tens of mT, although thermal demagnetization appears more efficient. To treat the remaining collection, a combination of a single heating (at 180 °C) and a subsequent stepwise AF demagnetization up to 50 mT was performed. A decent PCA component could not always be obtained, due to the noise which rapidly overcomes the NRM signal after a few demagnetization steps. In that case, the average direction obtained in the 10–20 mT range was used.

Due to the very low content of remanence-bearing mineral, most techniques of magnetic mineralogy were inappropriate, as shown by purely diamagnetic to paramagnetic magnetization curves (Fig. S7=mmc7). Two stronger magnetic samples (at a height of 24 and 30 m) yield consistent Pseudo-Single Domain (PSD) magnetite-like loops with $Mrs/Ms = 0.15$, $Bcr/Bc = 2.2$, Bcr from 22 to 27 mT, and Sratio of 0.96. Dominance of PSD magnetite is confirmed by the maximum unblocking temperature near 580 °C and median destructive field of NRM and IRM in the 20–50 mT range. In the Upper Travertine section, Isothermal Remanent Magnetization (IRM) at saturation is $\sim 1.5 \cdot 10^{-6}$ $A\,m^2\,kg^{-1}$ (Fig. 3), indicating a magnetite content in the order of 0.1 ppm. In the Upper Travertine and the lower formations, about 10% and 17% of IRM intensity remains after a 100 mT AF demagnetization, respectively. In the Upper Travertine and conglomerate formations, the Sratio (IRM in 3 T) varies between 0.93 and 0.98, while it varies between 0.78 and 0.85 in the lower formation. Combined with the few back-field magnetization curves (Fig. S7=mmc7), this confirms that magnetite is the sole magnetic carrier in the upper formations, while it dominates in the lower formation, mixed with a minor contribution of higher coercivity minerals like goethite and hematite. Whether this PSD magnetite is of volcanic and/or pedogenetic origin (wind-blown from regional soils and volcanic deposits) or biogenic origin (linked to bacterial activity specific to travertine formation) cannot be decided. Due to the rather instantaneous lithification of the sediment linked to travertine carbonate precipitation, we consider the ChRM direction yielding a reliable record of the geomagnetic field very soon after deposition.

As shown by the computed VGP latitude versus depth (Fig. 6), a reverse polarity strongly dominates except in the upper fluvio-lacustrine (Upper Conglomerates) section B where polarity is normal apart from the lower three samples, still within the Upper Travertine unit. Therefore the polarity change appears to coincide with the unconformity. Time lag corresponding to this unconformity is probably low due to the lack of paleosoil at the contact of the preserved travertine growth morphologies. The four top travertine sampled sites yield reverse polarity. Within the reverse polarity section, a few samples exhibit positive VGP latitudes, mostly near 30–35 m. To confirm that these data may correspond to the partial record of a short normal excursion, this interval was laterally re-sampled in an adjacent wall from the same quarry, distant from only 30 m and with continuous outcropping. These additional samples yield consistent reverse polarity. Therefore the initial suspected normal polarity probably results from poor quality measurements in this low intensity part or from remagnetization linked to water circulation in an open neotectonic fault observed close to the samples. Moreover, these samples were the first to be drilled in the mission, with a drill bit that appeared to be defectuous leading to poor quality and very short cores, thus suggesting possible sampling artefacts. Finally, section C, corresponding to a thicker lateral continuation of section B, yields reverse polarity except the lowest sample. As only the upper part of the section was sampled (due to unconsolidated and coarse material), we conclude that the normal polarity observed in section B is bracketed within reverse polarities. A conservative magnetostratigraphic interpretation is thus to place all the studied sections in the Matuyama chron and match the fluviatile B section with a short normal sub-chron within Matuyama. An alternative would be to place the normal polarity of section B above the reverse polarity of section C, possibly leading to a

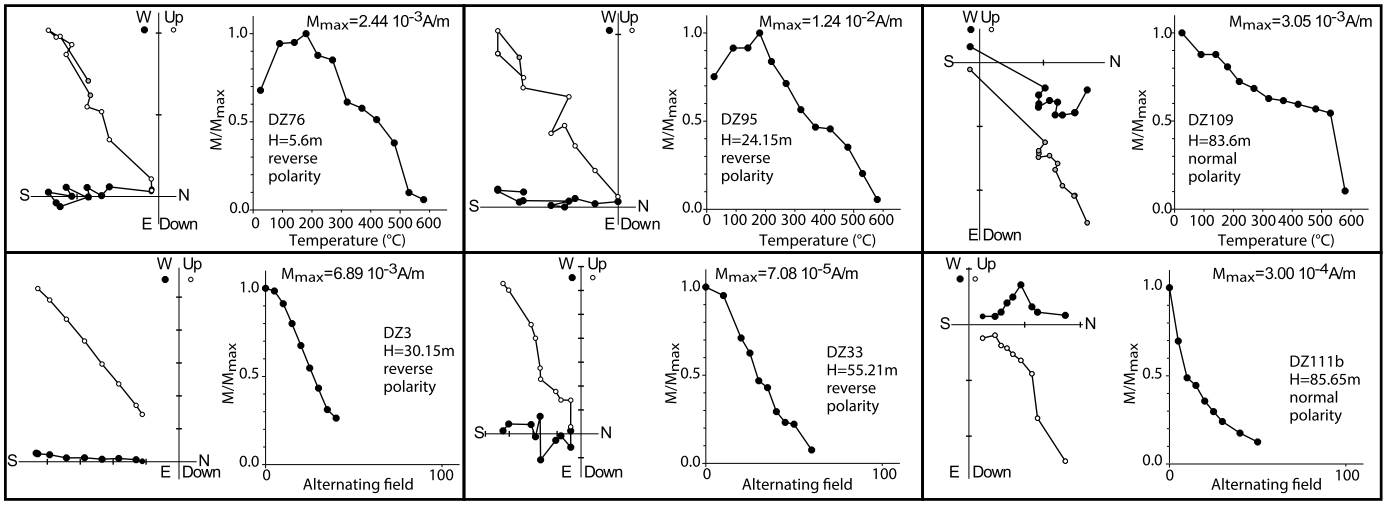

Fig. 5. Representative examples of thermal and AF demagnetization of NRM. Orthogonal projections (Zijderveld, 1967) and intensity decay curves for representative samples subject to thermal and alternating field demagnetization. On the orthogonal projection plots, open and solid circles represent projections on vertical and horizontal planes, respectively.

Bruhnes age for the top of section B. This alternative matches the 20 meters of fluviatile sediments sampled in section C with the three meters of unsampled marls at the base of section B. Moreover, it neglects the single sample with normal polarity at the base of C section. This hypothesis implies an extreme unlikely ad hoc combination of deposition rate fluctuation and sampling hiatus.

5.2. Cosmogenic nuclides

The model without post-burial production applied considering the thickness of the overlying material to the four samples from the deeply buried Lower Conglomerates (Fig. 1(b); Fig. S5=mmc5 (a), (b) and (c)) yields minimum burial ages ranging from 1.79 ± 0.15 Ma to 3.30 ± 1.05 Ma and denudation rates ranging from 3.8 ± 1.2 m Ma^{-1} to 9.7 ± 0.9 m Ma^{-1} (Table 1). Similarly, the exposure-burial diagram states none post-burial production and the minimum burial ages as well as the denudation rates determined using the ^{26}Al/^{10}Be versus ^{10}Be diagram that range from 1.63 Ma to 2.76 Ma (Fig. 4, Table 1) and from 4 m Ma^{-1} for DZ-Be-2 to ~9.9 m Ma^{-1} for the three others, respectively, are consistent with the values obtain performing the model without post-burial production. Taking into account possible post-burial production applying the post-burial production model to these four deeply buried Lower Conglomerates samples yield to remarkably similar maximized burial ages and denudation rates ranging from 1.78 ± 0.15 Ma to 3.31 ± 1.05 Ma and from 4.4 ± 0.8 m Ma^{-1} to 11.1 ± 0.6 m Ma^{-1}, respectively (Table 1). Regardless of the procedure used, the burial age and denudation rate estimates are internally consistent for all the samples from the Lower Conglomerates but DZ-Be-2, which may have experienced, and thus recorded, a different exposure, sedimentary and/or erosive history as demonstrated by the significantly different denudation rates associated with this peculiar sample. It may thus most likely have been definitively buried with a significantly lower initial ^{26}Al/^{10}Be concentration ratio compared to the three other samples.

Samples from sections B and C of the Upper Conglomerates (Fig. 1(c), (e), Fig. S5=mmc5 (a), (d) and (e)) yield: (1) minimum burial ages ranging from 1.23 ± 0.15 Ma to 1.65 ± 0.24 Ma and denudation rates ranging from 10.8 ± 0.7 m Ma^{-1} to 54.0 ± 7.7 m Ma^{-1} using the model without post-burial production (Table 1); (2) minimum burial ages ranging from 1.00 Ma to 1.41 Ma (Fig. 4, Table 1) and denudation rates ranging from 10 m Ma^{-1} to 53 m Ma^{-1} using the ^{26}Al/^{10}Be versus ^{10}Be diagram; (3) maximized burial ages ranging from 1.44 ± 0.11 Ma to 1.97 ± 0.15 Ma and denudation rates ranging from 9.8 ± 0.7 m Ma^{-1} to 60.4 ± 8.6 m Ma^{-1} using the post-burial production model (Table 1). Again, burial ages are internally consistent for all samples from the Upper Conglomerates. Regarding the denudation rates, the samples collected along section B lead to similar values. Four samples along section C yield again to internally consistent denudation rates intermediate between those derived from the sections A and B samples. The largest denudation rate derived from the DZ-Be-16 sample may reflect a different exposure, sedimentary and/or erosive history.

Due to the sampling depths, the nuclide post-burial production is limited for the Lower Conglomerates (~1%) but significant for the Upper Conglomerates (between 9 and 36%) (Table 1). A Chi^2 test (Ward and Wilson, 1978) applied to the Lower Conglomerates burial ages obtained using the two numerical models confirms that they all belong to the same population and thus allows calculating an inverse-variance weighted mean burial age of 1.96 ± 0.07 Ma. Considering the individual ages and their associated uncertainties, the Lower Conglomerates burial age is older than 1.63 Ma (obtained by subtracting it uncertainty to the youngest age [DZ-Be-8], that is $1.78 - 0.15 = 1.63$), the youngest minimum burial age also deduced from the exposure-burial diagram (Fig. 4, Table 1).

Chi^2 tests (Ward and Wilson, 1978) on the Upper Conglomerates burial ages obtained using the two numerical models were performed on the two spatially clustered sample groups (sections B and C, Fig. 1(c) and (e)). The chi^2 test on section B identifies the DZ-Be-4 burial age deduced from the post-burial production model (Table 1; 1.93 ± 0.17 Ma) as an outlier (Fig. 1(c) and (d)). An inverse-variance weighted mean burial age of 1.41 ± 0.04 Ma is calculated from the remaining values. The chi^2 test on the three upper samples of section C identifies DZ-Be-12 and DZ-Be-14 burial ages deduced from the post-burial production model (Table 1; 1.97 ± 0.15 Ma and 1.91 ± 0.12 Ma, respectively) as outliers (Fig. 1(e)). An inverse-variance weighted mean burial age of 1.43 ± 0.06 Ma is calculated from the remaining values. The two remaining samples from section C, i.e. DZ-Be-15 and DZ-Be-16, respectively ~10 and ~17 m deeper than the previously discussed samples, yield to, arithmetical means combining the minimum and maximum burial ages of the models of 1.48 ± 0.16 Ma for DZ-Be-15 and of 1.64 ± 0.33 Ma for DZ-Be-16. All the mean burial ages derived from the Upper Conglomerates

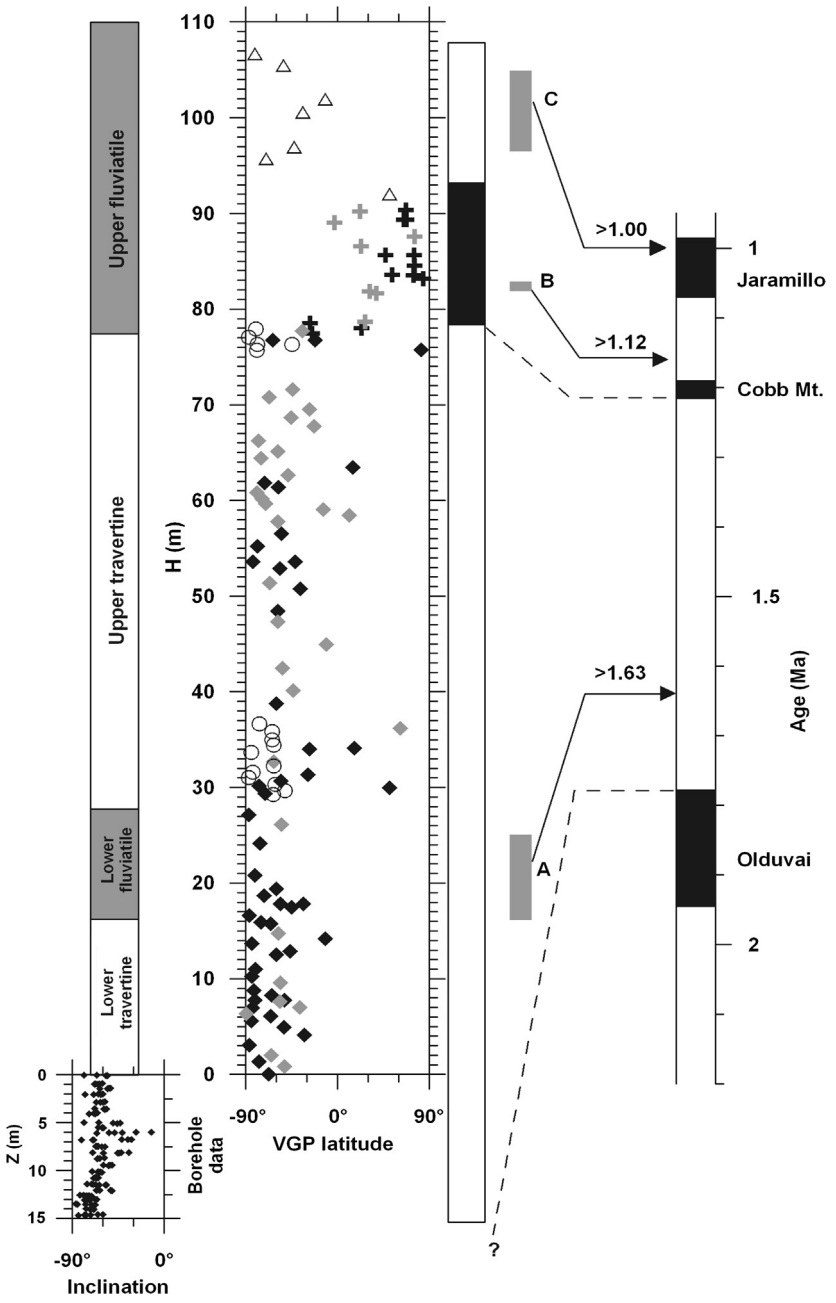

Fig. 6. Characteristic paleomagnetic directions (either VGP latitude for surface samples or inclination for borehole samples) as a function of synthetic stratigraphic height from the bottom of the quarry, together with proposed correlation with the GPTS (Laj and Channell, 2007) and cosmogenic nuclides results. Data from sections A, B, and C (Fig. 1) are represented with diamond, crosses and triangles, respectively. Circles indicate 2012 re-sampling from section A as well as two new outcrops from the top of the travertine. Black and gray symbols for sections A and B correspond to ChRM obtained by PCA or the simple directional average over the 180 °C and 10–20 mT demagnetization steps. The gray rectangles represent the cosmogenic sampling parts. They extend in the Lower Conglomerates section A between the heights of 16.3 and 25 m, in the Upper Conglomerates section B between the heights of 82.2 and 82.6 m, in the Upper Conglomerates section C between the heights of ~96 and 105 m, samples DZ-Be12 to DZ-Be-15 lying in an inverse polarity part. The minimum burial ages of 1.00 Ma and 1.12 Ma have been deduced from the exposure-burial diagram (Fig. 4, Table 1) and the minimum burial age of 1.63 Ma has been deduced both from the exposure-burial diagram and from the youngest age of the series subtracting its uncertainty (Fig. 4, Table 1). A, B and C refer to the sections A, B and C in Fig. 1.

samples are therefore internally consistent. Considering the section B individual ages and their associated uncertainties, the Upper Conglomerates burial age is older than 1.17 Ma (obtained by subtracting its uncertainty to the youngest age [DZ-Be-3], that is $1.27 - 0.10 = 1.17$), the youngest minimum burial age deduced from the exposure-burial diagram being 1.12 Ma (Fig. 4, Table 1). The section C Upper Conglomerates burial age is older than 1.08 Ma (obtained by subtracting its uncertainty to the youngest age [DZ-Be-13] from section C, that is $1.23 - 0.15 = 1.08$), the youngest minimum burial age deduced from the exposure-burial diagram being 1.00 Ma (Fig. 4, Table 1). Considering the potential influence of post-burial production at the relatively shallow sampling depth of the Upper Conglomerates samples that may maximize the calculated burial ages, these values of 1.00 Ma and 1.12 Ma will be further considered for the discussion.

The denudation rates derived from both the numerical models and the exposure-burial diagram are within the range of the denudation rates reported for the Mediterranean basin (e.g.: Brocard et al., 2003; Siame et al., 2004; Molliex et al., 2013).

6. Discussion and conclusions

The burial ages calculated for the Lower Conglomerates recording reverse polarity are compatible with deposition either just after or just before the Olduvai sub-chron. The second hypothesis is less likely as it implies that this sub-chron has not been recorded. Therefore, a preferred interpretation places the base of the studied section at an age younger than 1.78 Ma, and older than 1.63 Ma. The burial ages calculated for the Upper Conglomerates recording normal polarity are fully compatible with deposition during the Cobb Mountain sub-chron starting at 1.22 Ma (Fig. 6). This interpretation implies a significant change of the minimum deposition rate. The Upper Travertine units would have been deposited at roughly 10 m per 100 ka, which agrees with the age range and thickness of the still active Pamukkale travertine formation, while the Upper Conglomerates would have been deposited at a threefold larger deposition rate (13 m in at most 35 ka). This rate change is, however, compatible with the change from travertine to fluvio-lacustrine deposition. An alternative interpretation would be to assign the normal polarity to the Jaramillo sub-chron, starting at 1.07 Ma. This implies a marginal overestimation of the youngest possible minimum burial age of the normal polarity Upper Conglomerates (1.00 Ma) and a lack of Cobb Mountain sub-chron clear record (although the Cobb mountain trace could marginally be matched with the positive VGP latitudes around 60 or 76 m). In that case the deposition rate of the Upper Conglomerates would be of the same order than the Upper Travertine one. Another possibility is the record of the Gilsa normal polarity event at 1.56 Ma (Laj and Channell, 2007), which is also compatible with the burial age range. However, based on the elusive character of the Gilsa event (a seldom observed short duration excursion instead of a well established sub-chron like the Cobb Mountain), this older alternative is not relevant. Finally, the proposal of a Bruhnes age for the normal polarity is clearly at odds with both the magnetostratigraphic correlation of B and C sections and the burial age of the upper conglomerate in B section.

The above interpretation constrains the deposition of the Upper Travertine fossiliferous layers to between 1.22 (1.07) Ma and ~1.5 Ma according to the Cobb Mountain (Jaramillo) hypothesis. As the interpretation suggests possible emplacement of the Upper Travertine section over up to eight 41 ka climatic cycles (e.g. Lisiecki and Raymo, 2005) we looked for a record of climatic oscillations within isotopic and magnetic proxies (Fig. 3). No clear cyclicity emerges, while no obvious hiatus in travertine formation were detected, possibly suggesting that this travertine unit was built up within a single climatic cycle. Therefore the age of the fossil-bearing travertine section is likely in the 1.1–1.3 Ma range, in perfect agreement with the late Villafranchian age inferred for the mammal fauna, although ages up to 1.7 Ma cannot be firmly exclude.

This age range is also in accordance with the anthropological analysis pointing toward the similarity between the fragmentary Kocabaş skull and African *Homo erectus* such as KNM-ER3733, OH9 and Bouri–Daka specimens dated to 1.65, 1.4–1.5 and 1 Ma, respectively (McDougall et al., 2012; Schwartz and Tattersall, 2003; Gilbert and Asfaw, 2008), clearly out of the Upper and Middle Pleistocene hominid variability. Comparisons with the Buia–Danakil skull (Abbate et al., 1998), when more data will become available, will be of particular interest since the Kocabaş, Bouri–Daka and Buia–Danakil specimens sharing strong anthropological affinities most likely coexisted over a wide geographical area (from Turkey to East Africa) around 1 to 1.2 Ma. Interestingly, the Kocabaş skull is synchronous with the initial peopling of Europe (Carbonell et al., 2008; Muttoni et al., 2010; Toro-Moyano et al., 2013) and represents the strongest evidence of *Homo erectus* in western Asia.

The Upper Travertine paleo-environment, characterized by abundant freshwater and swamp like vegetation within dry surrounding limestone hills, is likely to have attracted the large thermophilic herbivores well represented in the paleontological record, as well as carnivores and early hominids following these abundant prey.

In remarkably close agreement with the latest biochronological estimations developed in this article, the cosmogenic nuclide burial dating and the associated paleomagnetic stratigraphy attest of the antiquity of the human occupation of the Anatolian Peninsula. These newly obtained chronological constraints challenge our current knowledge of the *Homo erectus* dispersal over the Old World.

Acknowledgements

The study was supported by international bilateral cooperation project between the Scientific and Technical Research Council of Turkey and the French Scientific Research National Center (CNRS) with research grant number of TUBITAK-CNRS 110Y335, and grant of RFBI 12-05-91372-ST_a. We are grateful to the Pernod–Ricard company which supports also this research program. M.C.A. thanks the grant of Outstanding Young Scientist Award from the Turkish Academy of Sciences (TUBA-GEBIP). We particularly thank Koray Ates and the logistic support of Faber Marble Group. S.M. thanks the Ege University projects TTM/001/2010, TTM/002/2011. We are deeply grateful to T. Tanju Kaya (Ege Univ. Natural Hist. Museum), for providing us all the comparative material from the Museum catalogue. The AMS measurements were performed thanks to the ASTER Team (M. Arnold, G. Aumaître, and K. Keddadouche) at the ASTER AMS national facility (CEREGE, Aix-en-Provence) that is supported by the INSU/CNRS, the French Ministry of Research and Higher Education, IRD and CEA. We also thank L. Leanni for her help during the chemical processing, Ph. Dussoulliez for artwork support, and N. Marriner for proof-reading the manuscript. The new reconstruction of the Kocabaş skull was done with the help of Patricia Wils from the French National Museum of Natural History. We acknowledge the patience and effort of the editor B. Marty in the reviewing process, as well as reviewers for their challenging questions and suggestions.

Appendix A. Supplementary material

Supplementary material related to this article can be found online at http://dx.doi.org/10.1016/j.epsl.2013.12.031.

References

Abbate, E., Albianelli, A., Azzaroli, A., Benvenuti, M., Tesfamariam, B., Bruni, P., Cipriani, N., Clarke, R.J., Ficcarelli, G., Macchiarelli, R., Napoleone, G., Papini, M., Rook, L., Sagri, M., Medhin Tecle, T., Torre, D., Villa, I., 1998. A one-million-year-old *Homo* cranium from the Danakil (Afar) Depression of Eritrea. Nature 393, 458–460.

Alçiçek, H., Varol, B., Özkul, M., 2007. Sedimentary facies, depositional environments and palaeogeographic evolution of the Neogene Denizli Basin of SW Anatolia, Turkey. Sediment. Geol. 202, 596–637.

Balco, G., Briner, J., Finkel, R.C., Rayburn, J.A., Ridge, J.C., Schaefer, J.M., 2009. Regional beryllium-10 production rate calibration for late-glacial northeastern North America. Quat. Geochronol. 4, 93–107.

Bar-Yosef, O., Belmaker, M., 2011. Early and Middle Pleistocene faunal and hominins dispersals through Southwestern Asia. Quat. Sci. Rev. 30, 1318–1337.

Bozkurt, E., 2001. Neotectonic of Turkey – a synthesis. Geodin. Acta 14, 3–30.

Braucher, R., Merchel, S., Borgomano, J., Bourlès, D.L., 2011. Production of cosmogenic radionuclides at great depth: A multi element approach. Earth Planet. Sci. Lett. 309 (1), 1–9.

Briner, J.P., Young, N.E., Goehring, B.M., Schaefer, J.M., 2012. Constraining Holocene ^{10}Be production rates in Greenland. J. Quat. Sci. 27, 2–6.

Brocard, G.Y., van der Beek, P.A., Bourlès, D.L., Siame, L.L., Mugnier, J.-L., 2003. Long-term fluvial incision rates and postglacial river relaxation time in the French Western Alps from ^{10}Be dating of alluvial terraces with assessment of inheritance, soil development and wind ablation effects. Earth Planet. Sci. Lett. 209, 197–214.

Carbonell, E., Bermúdez de Castro, J.M., Parés, J.M., Pérez-González, A., Cuenca-Bescós, G., Ollé, A., Mosquera, M., Huguet, R., van der Made, J., Rosas, A., Sala, R., Vallverdú, J., García, N., Granger, D.E., Martinón-Torres, M., Rodríguez, X.P., Stock, G.M., Vergès, J.M., Allué, E., Burjachs, F., Cáceres, I., Canals, A., Benito, A., Díez, C., Lozano, M., Mateos, A., Navazo, M., Rodríguez, J., Rosell, J., Arsuaga, J.L., 2008. The first hominin of Europe. Nature 452, 465–470.

Chmeleff, J., von Blanckenburg, F., Kossert, K., Jackob, D., 2010. Determination of the ^{10}Be half-life by multicollector ICP-MS and liquid scintillation counting. Nucl. Instrum. Methods Phys. Res., Sect. B, Beam Interact. Mater. Atoms 268, 192–199.

Engin, B., Güven, O., Köksal, F., 1999. Electron spin resonance age determination of a travertine sample from the southwestern part of Turkey. Appl. Radiat. Isot. 51 (6), 689–699.

Erten, H., Sen, S., Okzul, M., 2005. Pleistocene mammals from travertine deposits of the Denizli basin (SW Turkey). Ann. Paléontol. 91 (3), 267–278.

Fenton, C.R., Hermanns, R.L., Blikra, L.H., Kubik, P.W., Bryant, C., Niedermann, S., Meixner, A., Goethals, M.M., 2011. Regional ^{10}Be production rate calibration for the past 12 ka deduced from the radiocarbon-dated Grotlandsura and Russenes rock avalanches at 69°N, Norway. Quat. Geochronol. 6, 437–452.

Gilbert, W.H., Asfaw, B., 2008. Homo erectus: Pleistocene evidence from the Middle Awash, Ethiopia. Univ. California Press.

Goehring, B.M., Lohne, Ø.S., Mangerud, J., Svendsen, J.I., Gyllencreutz, R., Schaefer, J.M., Finkel, R.C., 2012. Late Glacial and Holocene beryllium-10 production rates for western Norway. J. Quat. Sci. 27, 89–96.

Granger, D.E., 2006. A review of burial dating methods using ^{26}Al and ^{10}Be. In: Siame, L.L., Bourlès, D.L., Brown, E.T. (Eds.), In Situ-Produced Cosmogenic Nuclides and Quantification of Geological Processes. In: Geological Society of America Special Papers, vol. 415, pp. 1–16.

Granger, D.E., Muzikar, P.F., 2001. Dating sediment burial with in situ-produced cosmogenic nuclides: theory, techniques, and limitations. Earth Planet. Sci. Lett. 188, 269–281.

Guipert, G., Vialet, A., de Lumley, M.A., de Lumley, H., 2012. Skull reconstruction of Barma del Caviglione 1, Grimaldi Caves, an Upper Paleolithic *Homo sapiens*. In: Annual Meeting of the American Association of Physical Anthropologists. Portland, USA, Am. J. Phys. Anthropol. 147, 157.

Hancock, P.L., Chalmers, R.M.L., Altunel, E., Çakır, Z., 1999. Travitonics: using travertines in active fault studies. J. Struct. Geol. 21, 903–916.

Kahlke, R.-D., Garcia, N., Kostopoulos, D., Lacombat, F., Lister, A., Mazza, P.P.A., Spassov, N., Titov, V.V., 2011. Western Palaearctic palaeoenvironmental conditions during the Early and early Middle Pleistocene inferred from large mammal communities, and implications for hominin dispersal in Europe. Quat. Sci. Rev. 30 (11–12), 1368–1395.

Kappelman, J., Alçiçek, M.C., Kazancı, N., Schultz, M., Özkul, M., Sen, S., 2008. First *Homo erectus* from Turkey and implications for migrations into temperate Eurasia. Am. J. Phys. Anthropol. 135, 110–116.

Korschinek, G., Bergmaier, A., Faestermann, T., Gerstmann, U.C., Knie, K., Rugel, G., Wallner, A., Dillmann, I., Dollinger, G., Lierse von Gostomski, Ch., Kossert, K., Maiti, M., Poutivtsev, M., Remmert, A., 2010. A new value for the ^{10}Be half-life by Heavy-Ion Elastic Recoil detection and liquid scintillation counting. Nucl. Instrum. Methods Phys. Res., Sect. B, Beam Interact. Mater. Atoms 268, 187–191.

Laj, C., Channell, J.E.T., 2007. Geomagnetic excursions. In: Kono, M. (Ed.), Treatise on Geophysics. In: Geomagnetism, vol. 15. Elsevier, Amsterdam, pp. 373–416.

Lisiecki, M.E., Raymo, L.E., 2005. A Pliocene–Pleistocene stack of 57 globally distributed benthic δ^{18}O records. Paleooceanography 20, PA1003. http://dx.doi.org/10.1029/2004PA001071.

de Lumley, H., Lordkipanidze, D., Féraud, G., Garcia, T., Perrenoud, C., Falguères, C., Gagnepain, J., Saos, T., Voinchet, 2002. Datation par la méthode ^{40}Ar/^{39}Ar de la couche de cendres volcaniques (couche VI) de Dmanisi (Géorgie) qui a livré des restes d'hominidés fossiles de 1, 81 Ma. C. R. Palevol 1 (3), 181–189.

McDougall, I., Brown, F.H., Vasconcelos, P.M., Cohen, B.E., Thiede, D.S., Buchanan, M.J., 2012. New single crystal ^{40}Ar/^{39}Ar ages improve time scale for deposition of the Omo Group, Omo–Turkana Basin, East Africa. J. Geol. Soc. Lond. 169, 213–226.

Molliex, S., Siame, L.L., Bourlès, D.L., Bellier, O., Braucher, R., Clauzon, G., 2013. Quaternary evolution of a large alluvial fan in a periglacial setting (Crau Plain, SE France) constrained by terrestrial cosmogenic nuclide (^{10}Be). Geomorphology 195, 45–52.

Muttoni, G., Scardia, G., Kent, D.V., 2010. Human migration into Europe during the late Early Pleistocene climate transition. Palaeogeogr. Palaeoclimatol. Palaeoecol. 296 (1–2), 79–93.

Nishiizumi, K., Winterer, E.L., Kohl, C.P., Klein, J., Middleton, R., Lal, D., Arnold, J.R., 1989. Cosmic ray production rates of ^{10}Be and ^{26}Al in quartz from glacially polished rocks. J. Geophys. Res. 94, 17907–17915.

O'Higgins, P., Jones, N., 2006. Tools for Statistical Shape Analysis. Hull York Medical School.

Pappu, S., Gunell, Y., Akhilesh, K., Braucher, R., Taieb, M., Demory, F., Thouveny, N., 2011. Early Pleistocene presence of Acheulian hominins in South India. Science 331, 1596–1599.

Rixhon, G., Braucher, R., Bourlès, D., Siame, L., Bovy, B., Demoulin, A., 2011. Quaternary river incision in NE Ardennes (Belgium) – Insights from ^{10}Be/^{26}Al dating of river terraces. Quat. Geochronol. 6 (2), 273–284.

Samworth, E.A., Warburton, E.K., Engelbertink, G.A.P., 1972. Beta decay of the ^{26}Al ground state. Phys. Rev. C 5, 138–142.

Schwartz, J.H., Tattersall, I., 2003. The Human Fossil Record, vol. 2. Craniodental Morphology of Genus *Homo* (Africa and Asia). Wiley Liss, New York.

Shen, G., Gao, X., Gao, B., Granger, D.E., 2009. Age of Zhoukoudian *Homo erectus* determined with ^{26}Al/^{10}Be burial dating. Nature 458, 198–200.

Siame, L., Bellier, O., Braucher, R., Sébrier, M., Cushing, M., Bourlès, D., Hamelin, B., Baroux, E., de Voogd, B., Raisbeck, G., Yiou, F., 2004. Local erosion rates versus active tectonics: cosmic ray exposure modeling in Provence (SE France). Earth Planet. Sci. Lett. 220, 345–364.

Şimşek, Ş., Günay, G., Elhatip, H., Ekmekçi, M., 2000. Environmental protection of geothermal waters and travertines at Pamukkale, Turkey. Geothermics 29, 557–577.

Stone, J.O., 2000. Air pressure and cosmogenic isotope production. J. Geophys. Res. 105 (B10), 23753–23759.

Sun, S., 1990. Denizli–Uşak Arasının Jeolojisi ve Linyit Olanakları (The Geology and Lignite Potential of Denizli–Uşak Region). Scientific Report N° 9985. General Directorate of the Mineral Research and Exploration of Turkey (MTA), Ankara. 92 pp.

Toro-Moyano, I., Martínez-Navarro, B., Agustí, J., Souday, C., Bermúdez de Castro, J.M., et al., 2013. The oldest human fosil in Europe dated to ca. 1.4 Ma at Orce (Spain). J. Hum. Evol. 65 (1), 1–9.

van der Made, J., Morales, J., 2011. *Mitilanotherium inexpectatum* (Giraffidae, Mammalia) from Huélago (Lower Pleistocene; Guadix–Baza basin Granada, Spain) – observations on a peculiar biogeographic pattern. Estud. Geol. 67, 613–627.

Vialet, A., Guipert, G., He, J., Feng, X., Lu, Z., Wang, Y., Li, T., de Lumley, M.-A., de Lumley, H., 2010. The *Homo erectus* from the Yunxian and Nankin Chinese sites. Anthropological improvements by using 3D virtual imaging technique. C. R. Palevol 9, 331–339.

Vialet, A., Guipert, G., Alçiçek, M.C., 2012. *Homo erectus* still further west. Reconstruction of the Kocabaş cranium (Denizli, Turkey). C. R. Palevol 11 (2–3), 89–95.

Ward, G.K., Wilson, S.R., 1978. Procedures for comparing and combining radiocarbon age determinations: a critique. Archaeometry 20, 19–31.

Westaway, R., 1993. Neogene evolution of the Denizli region of western Turkey. J. Struct. Geol. 15, 37–53.

Zijderveld, J.D.A., 1967. Demagnetization analysis of results. In: Methods in Paleomagnetism. Elsevier, Amsterdam, pp. 254–286.